BASOLATERAL SORTING OF CHLORIDE CHANNEL 2 IS MEDIATED BY INTERACTIONS BETWEEN A DILEUCINE MOTIF AND THE CLATHRIN ADAPTOR AP-1

Erwin de la Fuente-Ortega *, †, ‡, ¶
Diego Gravotta *, †, ¶
Andres Perez Bay †
Ignacio Benedicto †
Jose Maria Carvajal-Gonzalez †, §
Guillermo Lehmann †
Carlos F. Lagos ⁊
Enrique Rodríguez-Boulan †, ¶

* Authors contributed equally.
† Dyson Vision Research Institute, Department of Ophthalmology, Weill Cornell Medical College, 1300 York Avenue, New York, NY 10065.
‡ Current address: Departamento de Ciencias Biomedicas, Facultad de Medicina, Universidad Católica del Norte, Larrondo 1281, Coquimbo, Chile.
§ Current address: Universidad de Extremadura, España.
⁊ Department of Endocrinology, School of Medicine, Pontificia Universidad Catolica de Chile, Lira 85, 5th floor, Santiago, Chile. Department of Endocrinology, School of Medicine, Pontificia Universidad Católica de Chile, Lira 85, 5th Floor, Santiago, Chile and Facultad de Ciencia, Universidad San Sebastián, Lota 2465, Providencia, Santiago, Chile.
¶ Corresponding authors. Email: boulan@med.cornell.edu, dig2003@med.cornell.edu, edelafuente@ucn.cl

Running title: Basolateral sorting of ClC2 mediated by AP-1.

SUMMARY

In spite of the many key cellular functions of chloride channels, the mechanisms that mediate their subcellular localization are largely unknown. ClC-2 is a ubiquitous chloride channel usually localized to the basolateral domain of epithelia that regulates cell volume, ion transport and acid-base balance; mice knocked-out for ClC-2 are blind and sterile. Previous work has suggested that CLC-2 is sorted basolaterally by TIFS^{812}LL, a dileucine motif in CLC-2's C-terminal domain. However, our *in silico* modelling of ClC-2 suggested that this motif was buried within the channel's dimerization interface and identified two cytoplasmically exposed dileucine motifs, ESMI^{623}LL and QVVA^{635}LL, as candidate sorting signals. Alanine mutagenesis and trafficking assays support a scenario in which ESMI^{623}LL acts as the authentic basolateral signal of ClC-2. Silencing experiments and yeast three hybrid assays demonstrated that both ubiquitous (AP-1A) and epithelial-specific (AP-1B) forms of the tetrameric clathrin adaptor AP-1 are capable of carrying out basolateral sorting ClC-2 through interactions of ESMI^{623}LL with a highly conserved pocket in their γ1-σ1A hemicomplex.

Supplemental Material can be found at:
http://www.molbiolcell.org/content/suppl/2015/03/02/mbc.E15-01-0047v1.DC1.html

INTRODUCTION

Chloride channels control a wide array of key cellular functions, e.g. muscle and nerve excitability, trans-epithelial salt and water transport, cell volume and acidification of intracellular organelles; not surprisingly, their mutations lead to a wide spectrum of human diseases (Jentsch *et al.*, 2005; Stölting *et al.*, 2014). ClC-2 is a ubiquitous voltage-gated chloride channel, particularly abundant in epithelial tissues (Gründer *et al.*, 1992; Thiemann *et al.*, 1992), believed to play key roles in trans-epithelial chloride transport processes in response to hyperpolarization, cell swelling and extracellular acidification (T. J. Jentsch, 2005). ClC-2 belongs to a family of 9 mammalian chloride channels: whereas ClC-2, ClC-1, ClC-Ka and ClC-Kb preferentially localize to the plasma membrane, the other family members, ClC-3, 4, 5, 6, 7 localize to endosomal compartments (Jentsch, 2008). ClC-2 knock-out in mice causes blindness and male sterility (Bosl *et al.*, 2001; Nehrke *et al.*, 2002; Edwards *et al.*, 2010) consistent with its expression in epithelial cells that form blood-tissue barriers in retina and testis, i.e. retinal pigment epithelium (RPE) and Sertoli cells (T. J. Jentsch, 2005; Strauss, 2005). Chloride channels are usually dimers, with each monomer having its own pore (Jentsch, 2002). Based on the crystal structure of structurally similar bacterial channels, ClC-2 is believed to be a polytopic protein, with 18 α-helical segments (A-R) and a large cytoplasmically exposed C-terminal segment containing two cystathionine β-synthase (CBS) domains, CBS1 and CBS2 (Peña-Münzenmayer *et al.*, 2005) (Figure 1A). Mutational studies and structural modeling suggest that the CBS domains modulate the trafficking and channel activity of ClC-2 (Peña-Münzenmayer *et al.*, 2005; Garcia-Olivares *et al.*, 2008; Feng *et al.*, 2010).

The polarized localization of ClC-2 in epithelial cells was initially controversial, with some studies reporting an apical localization in lung alveolar cells (Murray *et al.*, 1995; Blaisdell *et al.*, 2000) and intestinal cells (Gyömörey *et al.*, 2000) that made it a good candidate to complement CFTR's secretory function and other studies reporting a basolateral localization in intestinal cells compatible with absorption processes (Catalan, Marcelo, Cornejo *et al.*, 2002; Lipecka *et al.*, 2002; Catalán *et al.*, 2004). However, a immunocytochemical and transfection study (Peña-Münzenmayer *et al.*, 2005) unequivocally established that ClC-2 localizes to the basolateral plasma membrane of absorptive epithelial cells of rat and mouse colon and small intestine. Furthermore, mutagenesis experiments by these authors identified a dileucine motif, TIFS^{812}LL, implicated in the basolateral localization of ClC-2 in MDCK cells and suggested a role of the clathrin adaptor AP-1B in the basolateral sorting of the channel.

Dileucine-based sorting signals fall into two main classes, defined by the consensus motifs DXXLL and [D/E]XXXL[L/I] (D, aspartate; E, glutamate; L, leucine; I, isoleucine). DXXLL motifs occur within the cytosolic tails of intracellular sorting receptors such as mannose-6-phosphate receptors (MPRs) (Johnson and Kornfeld, 1992) and are known to bind to the Vps27, Hrs and Stam (VHS) domain of Golgi-localized, γ-ear-containing, ARF-binding proteins (GGAs) (Puertollano *et al.*, 2001; Zhu *et al.*, 2001). [D/E]XXXL[L/I] motifs (Letourneur and Klausner, 1992) are present in the cytoplasmic domains of many transmembrane proteins targeted to endosomes, lysosomes and lysosome-related organelles (Bonifacino and Traub, 2003). Both types of dileucine motifs are known to participate in clathrin-mediated post-Golgi sorting of membrane proteins to endosomes and lysosomes (Bonifacino and Traub, 2003; Traub,

2009). Furthermore, [D/E]XXXL[L/I] motifs have been implicated in clathrin-mediated endocytosis (Letourneur and Klausner, 1992) and, relevant to this paper, in the post-Golgi sorting of about a dozen basolateral proteins (Table 1). In [D/E]XXXL[L/I] motifs, the leucine-leucine and leucine-isoleucine pairs are critical elements of the signals, whereas the aspartate or glutamate residue at the -4 position is often important but not essential for function (for examples of both cases, see Table 1). Yeast three hybrid and GST-protein pull down assays have shown that [D/E]XXXL[L/I] motifs interact with the γ–σ1 hemicomplex of the heterotetrameric clathrin adaptor AP-1 (Janvier *et al.*, 2003a; Doray *et al.*, 2007) through conserved residues also present in the equivalent α–σ2 a δ–σ3 hemicomplexes of the clathrin adaptors AP-2 and AP-3 (Kelly *et al.*, 2008; Mattera *et al.*, 2011). Furthermore, it is now clear that AP-1 occurs as a diversity of heterotetramers through combinatorial assembly of various γ and σ1 subunits, encoded by different genes. Relevant to this paper, γ subunits occur as two variants, γ1 and γ2; heterotetramers containing the former bind to a broad range of [D/E]XXXL[L/I] motifs whereas heterotetramers containing the latter are specific for a small number of [D/E]XXXL[L/I] motifs present largely in proteins targeted to the melanosome (Kelly *et al.*, 2008; Mattera *et al.*, 2011).

A key aspect in the characterization of a basolateral sorting mechanism is the identification of the sorting adaptor involved. It is now clear that AP-1 and clathrin are key regulators of basolateral protein sorting (Deborde *et al.*, 2008; Gonzalez and Rodriguez-Boulan, 2009; Bonifacino, 2014; Nakatsu *et al.*, 2014); one publication supports that AP-4 also regulates basolateral sorting (Hunziker and Fumey, 1994). The epithelial-specific variant of AP-1, AP-1B, was initially shown to mediate basolateral sorting (Fölsch *et al.*, 1999; Ohno *et al.*, 1999; Gan *et al.*, 2002; Gravotta *et al.*, 2007). AP-1A, the ubiquitous form of AP-1, possesses a different medium subunit (μ1A instead of μ1B, 85% identity) and was recently shown to also mediate basolateral protein sorting (Carvajal-Gonzalez et al., 2012; Gravotta et al., 2012). Both AP-1A and AP-1B were shown to interact with tyrosine-based basolateral sorting signals (Yxxϕ) via pockets in their μ1A and μ1B subunits, structurally similar to the pocket found in the μ2 subunit of AP-2 (Carvajal-Gonzalez *et al.*, 2012). In contrast, the role of clathrin adaptors in the sorting of basolateral proteins with dileucine-based basolateral sorting signals has not been studied in depth (Table 1). A publication supports a role of the clathrin machinery in the sorting of intracellular chloride channels (e.g. ClC-3, 4, 5, 6 and 7) (Stauber and Jentsch, 2010), but the role of clathrin adaptors in the sorting of plasma membrane chloride channels remains completely unknown. A decade-old study suggested that basolateral sorting of ClC-2 was mediated by AP-1B, but not by AP-1A, (Peña-Münzenmayer *et al.*, 2005) but did not characterize the interactions between channel and adaptors.

Here, we combined *in silico* modeling, trafficking studies and yeast 3 hybrid assays to study in detail the mechanisms involved in the basolateral sorting of ClC-2 in MDCK cells. Our experiments demonstrate that two dileucine motifs, ESMI^{623}LL and QVVA^{635}LL, different from the one previously postulated (Peña-Münzenmayer *et al.*, 2005), mediate basolateral sorting of ClC-2, and define specific interactions with the γ1–σ1 hemicomplex present in both AP-1A and AP-1B required for basolateral localization of the channel.

RESULTS

In silico molecular model of ClC-2.

The human chloride channel 2 (ClC-2) is a polytopic plasma membrane protein with 18 α-helices presumed to cross the bilayer and with both N- and C-terminal domains facing the cytoplasm (Dutzler *et al.*, 2002; Peña-Münzenmayer *et al.*, 2005; Feng *et al.*, 2010) (Figure 1A). ClC-2 displays three distinct potential di-leucine motifs in its C-terminus domain: ESMI^{623}LL and QVVA^{635}LL within CBS-1, and TIFS^{812}LL within CBS-2 (Peña-Münzenmayer *et al.*, 2005) (Figure 1A). These motifs are highly conserved throughout evolution, with the exception of QVVA^{635}LL, which in birds displays a methionine instead of a leucine (QVVA^{645}ML) (Figure 1B).

In order to obtain insights on the structural environment of ESMI^{623}LL, QVVA^{635}LL and TIFS^{812}LL motifs that might help define their possible role in basolateral sorting, we built an *in silico* molecular model of ClC-2 based on the reported crystal structures of the eukaryote channel CmClC (Feng *et al.*, 2010) and the C-terminus segments of mammalian ClC-Ka and ClC-0 (Markovic and Dutzler, 2007a). Although current crystallographic evidence for the C-terminus domain of human ClCs does not allow a complete structural characterization, the available crystal structures for the cytoplasmic C-terminal domains of ClC-0, ClC-Ka and ClC-5 demonstrate that, within each monomer, CBS domains form dimeric Bateman modules which in turn dimerize to form the quaternary structure of the ClC channel's cytoplasmic domain (Strange, 2011). The 3D model of ClC-2 we obtained (Figure 1, C and D and Video 1) highlights the positions of the three dileucine motifs in ClC-2 within the context of the monomeric and dimeric configurations of the channel (Figure 1D). Surprisingly, given that TIFS^{812}LL was postulated to be a basolateral sorting signal of ClC-2, the model revealed that TIFS^{812}LL has limited structural exposure as it appear located within a region of CBS-2 sandwiched between the two monomers (Figure 1D and Video 1). In contrast, the model predicts that ESMI^{623}LL and QVVA^{635}LL, both in the CBS1 domain, displayed a better structural exposure. ESMI^{623}LL appears integrated into a conserved sheet-loop-sheet secondary structure within CBS1 that forms an interface with CBS2 (Figure 1C), a feature common to other members of the ClC family. The calculated total values of solvent accessibilities of residues and of residue-side chains, derived from this model, were 1.4 times higher for ESMI^{623}LL relative to QVVA^{635}LL or TIFS^{812}LL (Table 2). Taken together, these two parameters , suggest that, among the three candidate dileucine motifs, ESMI^{623}LL has the highest cytoplasmic accessibility .

The basolateral distribution of ClC-2 is abrogated by mutagenesis of ESMI^{623}LL or QVVA^{635}LL but not TIFS^{812}LL motifs.

The analyses of the cytoplasmic accessibility of the three dileucine motifs in our *in silico* model of ClC-2 predicted that ESMI^{623}LL and to a lesser extent QVVA^{635}LL were more likely basolateral sorting signals than TIFS^{812}LL. Since this finding contradicts a previous report (Peña-Münzenmayer *et al.*, 2005), we carried out a

systematic study to dissect the individual roles of these dileucine motifs in the polarized trafficking on ClC-2 in MDCK cells.

To this end, we selectively mutated the leucine pairs in each dileucine motif to alanines in the context of ClC-2 harboring a HA epitope-tag in its luminal domain (HA-ClC-2, Figure 2A) (kindly provided by Dr. Francisco Sepulveda, CECs, Chile) and studied the distribution of wild type and mutant HA-ClC-2 in stably transfected MDCK cell lines. In agreement with Peña-Münzenmayer et al., we found that wild type HA-ClC-2 localized preferentially to the basolateral membrane (Figure 2, B and C). In contrast with their findings, however, we found that HA-ClC-2[^{812}LL/AA] localized basolaterally in MDCK cells, exactly as wild type HA-ClC-2 (Figure 2, B and C). Importantly, in agreement with the predictions of our structural model of ClC-2, immunolabeling of surface and total pools of HA-ClC-2[^{623}LL/AA] and HA-ClC-2[^{635}LL/AA] indicated that these proteins displayed a predominantly intracellular localization (Figure 2B), consistent with a possible sorting signal role of ESMI^{623}LL and QVVA^{635}LL. The strong intracellular retention caused by disruption of either ESMI^{623}LL or QVVA^{635}LL motifs was previously observed in non-polarized cells (Peña-Münzenmayer *et al.*, 2005; Cornejo *et al.*, 2009).

To further dissect the possible basolateral sorting roles of ESMI^{623}LL and QVVA^{635}LL, we transplanted the cytoplasmic C-terminus domain of ClC-2 to a reporter molecule, p75 neurotrophin receptor (p75NTR), an approach that we have previously used to simplify the analysis of the trafficking signals for basolateral proteins, particularly those with multiple membrane spanning domains (Figure 2D) (Le Gall *et al.*, 1997; Castorino *et al.*, 2011). Experiments carried out with these chimeras expressed in stable MDCK cell lines showed that p75-ClC-2ct (WT) and p75-ClC-2ct [^{812}LL/AA] had a normal basolateral localization whereas p75-ClC-2ct[^{623}LL/AA] and p75-ClC-2ct[^{635}LL/AA] were predominantly localized to the apical membrane (Figure 2E). Why would these mutations cause intracellular retention of the full size channel and apical localization of the chimeric proteins ? A parsimonious interpretation is that, unlike p75NTR (Yeaman *et al.*, 1997), the full size channel has no strong apical signals that might promote its apical expression in the absence of basolateral sorting signals (see Discussion for further analysis of this point).

Two major conclusions may be drawn from these experiments. First, TIFS^{812}LL does not act as a basolateral sorting signal for ClC-2. Second, ESMI^{623}LL and QVVA^{635}L are involved in the basolateral sorting of ClC-2 but are not able to act as independent basolateral signals, as they do not show evidence of redundancy. We hypothesize that only one of these two motifs is the authentic basolateral sorting signal while the other one plays a structural role in CBS1 that supports the sorting signal function of the other motif. The following experiments were designed to test this hypothesis.

ESMI^{623}LL is the authentic basolateral sorting signal of ClC-2.

Collectively the information provided by the *in silico* model of ClC-2 and the mutagenesis experiments described above suggested that ESMI^{623}LL and QVVA^{635}LL contribute to the basolateral sorting signal of ClC-2. To collect additional evidence that would allow us to determine which motif functions as the authentic basolateral signal of ClC-2, we carried out mutagenesis of individual residues in each of the two motifs to

dissect their individual contribution to the basolateral localization of ClC-2, after transient expression of the mutant proteins into polarized MDCK cells. Cell surface and total HA-ClC-2 was determined by sequentially immunolabeling the luminal HA-epitope, in intact cells and after cell permeabilization, with two different species of anti-HA antibodies (Figure 3A). Representative images of confocal sections derived from these experiments are shown in Figure 3B. Data obtained from quantification of these experiments were expressed as fractional distribution of surface versus intracellular HA-ClC-2 (Figure 3C) and analyzed for statistical significance using ANOVA and Bonferroni's T-test corrections (Figure 3C and supplemental Table S1).

We observed that HA-ClC-2 localized predominantly to the plasma membrane (0.80 ± 0.03), with a small fraction retained intracellularly (0.20 ± 0.03) (Figure 3, B and C). In contrast, most of HA-ClC-2[^{623}L/A] was localized intracellularly (0.72 ± 0.02) with only a small fraction at the cell surface (0.28 ± 0.02) representing a 64% reduction and a 350% increase in the surface and intracellular distributions, respectively (Figure 3, B and C and statistical analyses in supplemental Table S1). Importantly, the localization of HA-ClC-2[^{624}L/A] was also significantly altered compared to that of HA-ClC-2 with approximately equal surface and intracellular pools (0.52 ± 0.02 and 0.48 ± 0.02, representing a 35% reduction and a 236% increase, respectively) (Figure 3, B and C; see statistical analyses in supplemental Table S1). Equivalent analysis of the QVVA^{635}LL motif indicated that the single mutants HA-ClC2[^{635}L/A] and HA-ClC2 [^{636}L/A] did not display significant intracellular retention (Figure 3, B and C; supplemental Table S1). Thus, since individual leucine mutagenesis of ESMI^{623}LL disrupted basolateral localization of ClC-2, we conclude that QVVA^{635}LL cannot mediate basolateral sorting as an independent basolateral signal. Furthermore, leucine mutagenesis of QVVA^{635}LL did not cause missorting of ClC-2, which is consistent with the idea that ESMI^{623}LL is the only basolateral signal of ClC-2.

To complete the characterization of ESMI^{623}LL as a basolateral sorting signal, we carried out alanine substitutions of the remaining residues and performed the localization assay described above. The mutants generated, HA-ClC-2[^{619}E/A], HA-ClC-2[^{620}S/A] and HA-ClC-2[^{622}I/A], were expressed in MDCK cells and their distribution quantified essentially as described in Figure 3A (Supplemental Figure S2). All mutants displayed similar surface and intracellular distributions as wild type HA-ClC-2 (Supplemental Figure S2, B and C; see statistical analyses in supplemental Table S3) indicating that, unlike ^{623}L and ^{624}L, the respective mutated residues were not required for basolateral sorting of ClC-2. Taken together, these experiments further strengthen the hypothesis that ESMI^{623}LL is the authentic basolateral sorting signal of ClC-2.

To validate these conclusions, obtained using a quantitative imaging approach in transiently transfected MDCK cells, we utilized an alternative biochemical approach. We generated a lentivus panel encoding all the individual leucine-alanine replacements and quantified apical, basolateral and intracellular distributions of HA-ClC-2 mutants in polarized infected MDCK cells using a previously described surface biotinylation avidin shift (SBAS) assay (Gravotta et al., 2012) (Supplemental Figure S4). Overall these experiments were in agreement with the observation in transient transfected cells

as they supported a signaling role for ESMI^{623}LL in the basolateral sorting of CLC-2 (Supplemental Table S1, and supplemental Table S5).

Since HA-ClC-2[^{623}L/A] failed to reach the surface and accumulated intracellularly we quantified the accumulation of this mutant at intracellular transit compartments. Quantification of the extent of colocalization with TGN38 and transferrin receptor (TfR), which are markers of the TGN and the endosomal compartment, respectively, showed a moderate steady-state increase of the mutant at the level of the TGN (Supplemental Table S6).

Clathrin adaptors AP-1A and AP-1B mediate basolateral sorting of ClC-2.

Next, we carried out experiments to identify the machinery that mediates basolateral trafficking of ClC-2. To date, both variants of the clathrin-adaptor AP-1, AP-1B (Fölsch *et al.*, 1999; Ohno *et al.*, 1999) and AP-1A (Carvajal-Gonzalez *et al.*, 2012; Gravotta *et al.*, 2012), have been implicated in basolateral sorting. These tetrameric adaptors share three subunits (β1, σ1 and γ1) and have different, albeit highly homologous (85%), medium subunits (μ1A and μ1B). Stable MDCK cells expressing HA-ClC-2 were treated with siRNAs against μ1A (A-KD), μ1B (B-KD), both μ1A and μ1B (AB-KD), or against luciferase (control, WT), and analyzed 10 days later; the siRNAs were previously characterized (Carvajal-Gonzalez et al., 2012; Gravotta et al., 2012) (Figure 4A). In singly silenced A-KD and B-KD cells, HA-ClC-2 localized predominantly to the basolateral membrane, a distribution similar to that displayed by WT MDCK cells. In contrast, MDCK cells in which both μ1A and μ1B were knocked-down (AB-KD) exhibited a drastic reduction (>50%) in surface localization and a corresponding increment (190%) in intracellular localization of the channel, compared to WT cells (Figure 4, B and C; statistical analysis in supplemental Table S7).

We further tested the roles of AP-1A and AP-1B in the sorting of ClC-2 in the context of the p75-ClC-2ct chimera (Figure 5). Stable MDCK cell lines expressing p75-ClC-2ct were subjected to silencing of μ1A and μ1B, as described above, and immunolabeled as described in Figure 3A using two different species of anti-p75 antibody to detect surface and total pool of chimeras (Figure 5A). In WT cells, p75-ClC-2ct was found preferentially at the basolateral membrane (0.43 ± 0.02) with a minor proportion at the apical membrane (0.02 ± 0.0062) (Figure 5, B and C; statistical analyses in supplemental Table S8). Similar basolateral distributions were determined for A-KD (0.52 ± 0.02) and B-KD (0.48 ± 0.01) cells (Figure 5, B and C; statistical analyses in supplemental Table S8). In contrast, AB-KD MDCK cells shifted a substantial fraction of p75-ClC-2ct towards the apical membrane (0.16 ± 0.02), significantly larger than that determined for WT cells (0.02 ± 0.006), increasing more than ten fold the AP/BL ratio from 0.05 in WT MDCK cells to 0.6 in AB-KD MDCK cells (Figure 5, B and C; statistical analyses in supplemental Table S8). Importantly, the intracellular fraction of ClC-2 remained the same in WT, A-KD, B-KD and AB-KD MDCK cells, suggesting that the presence of strong apical signals in p75 was sufficient to prevent intracellular accumulation of the chimeric proteins upon removal of the adaptors that recognize ClC-2's basolateral signal (Figure 5D).

Taken together, these experiments indicated that the presence of either AP-1A or AP-1B variants of AP-1 is sufficient to generate and maintain a basolateral

distribution of ClC-2.

ESMI^{623}LL but not TIFS^{812}LL interacts with γ1–σ□□ hemicomplex of AP-1.
Collectively, the evidence discussed above reveals that ClC-2 utilizes the dileucine motifs ESMI^{623}LL or QVVA^{635}LL as a basolateral sorting signal and requires either AP-1A or AP-1B for basolateral localization in polarized MDCK cells. If these conclusions are correct, we might expect to detect direct interactions between one of the two dileucine motifs and both adaptors, using a yeast three-hybrid (Y3H) assay. To this end, we carried out Y3H assays using the 347 amino acid C-terminal cytoplasmic domain of ClC-2 and the γ1–σ□□ hemicomplex, present in both AP-1A and AP-1B. As positive control we used the HIV Nef (NLA4-3 variant) protein, which displays a canonical, dileucine motif (ENTSLL) that mediates selective interaction with γ1–σ□□ (AP-1) and δ–σ3A □□□□□□ but not with α–σ□ (□□□□) (Janvier *et al.*, 2003b; Doray *et al.*, 2007) . Qualitative and quantitative forms of the Y3H assay (plate and liquid growth, respectively, see details in Materials and Methods) revealed that wild type ClC-2ct interacted specifically with the γ1–σ□□ hemicomplex, albeit with less avidity than Nef (Figure 6, A and B)□ Importantly, alanine substitution of both leucine residues in TIFS^{812}LL had no effect on this Y3H interaction; in contrast, double alanine substitution in either ESMI^{623}LL or QVVA^{635}LL abrogated the interaction with γ1–σ□□ (Figure 6, A and B). These observations are in close agreement with the alanine mutagenesis/trafficking experiments described in Figure 2, which suggested that either ESMI^{623}LL or QVVA^{635}LL but not TIFS^{812}LL were candidate basolateral sorting signals for the channel. Furthermore, they agree with our hypothesis that these two motifs do not behave as independent basolateral sorting signals for the channel.

In order to obtain additional evidence for the sorting signal activity of ESMI^{623}LL or QVVA^{635}LL, we studied the Y3H interaction between the ClC-2 C-terminal domain with single alanine substitutions in ESMI^{623}LL or QVVA^{635}LL and the γ1–σ□□ hemicomplex. Strikingly, these experiments revealed that both mutations in ESMI^{623}LL, L623A and L624A, disrupted the interaction with γ1–σ□□ (Figure 6, C and D) compatible with an authentic basolateral signal role for this dileucine motif. In contrast, mutation of only one of the leucines in QVVA^{635}LL, L636A or L636S but not of the other one, L635A or L635S, inhibited the Y3H interaction of ClC-2ct with the γ1–σ□□ hemicomplex, inconsistent with the expected behavior of an authentic dileucine sorting motif. A similar strategy to test the interaction of the remaining residues in both dileucine motifs revealed no or minimal roles of the residues at position -4 (^{619}E or ^{631}Q), -2 and -1 (Figure 6, E and G).

In summary, in close agreement with the trafficking experiments described earlier that prioritized ESMI^{623}LL over QVVA^{635}LL as a candidate basolateral signal, the Y3H experiments in this section indicate that the interaction of ESMI^{623}LL with the γ1–σ□□ complex is more typical of a cognate dileucine motif than that of QVVA^{635}LL.

Mutations in the highly conserved γ1–σ□□ pocket of AP-1 disrupt interaction with the basolateral signal of ClC-2

Crystallographic analysis of the α–σ2 hemicomplex of AP-2 and peptides containing the dileucine motif has identified residues in the hydrophobic pocket, e.g. ^{65}L, ^{88}V and ^{98}V in the σ2 subunit, that accommodate the dileucine motif (Kelly *et al.*, 2008). More recently, equivalent residues in the subunit σ1 of AP-1, ^{63}A and ^{88}V, have been found to interact with Nef's ENTSLL (Mattera *et al.*, 2011). Based on these previous observations, we modeled *in silico* the interaction between the basolateral signal of ClC-2, ESMI^{623}LL, and AP-1's hemicomplex γ1–σ□□. The model suggested important interactions with key conserved residues in σ□□. In particular it suggested that ^{623}L in ClC-2 binds to a hydrophobic pocket constituted by the side chains of residues ^{63}A, ^{65}L, ^{88}V and ^{98}V in σ□□ (Figure 7A). An additional hydrophobic interaction (H-bonds) may occur between the nitrogen amide of ^{623}L in ClC-2 and a carboxyl group of ^{98}V in σ□□. A second hydrophobic pocket, generated by the side chains of ^{62}Y and ^{88}V in σ□□, is predicted to accommodate the side chain of ^{624}L in ClC-2. The model suggests hydrogen bonding between side chains of ^{621}M in ClC-2 and ^{63}A in σ□□, between the side chain of ^{64}S in σ□□ and ^{618}P in ClC-2 and between the carboxyl group of ^{619}E in ClC-2 and backbone nitrogens of ^{100}E and ^{101}L in σ□□. It also suggests that the carboxyl group of ^{619}E in ClC-2 establishes extensive polar interactions with side chains of ^{15}R in σ□□ and ^{15}R in γ1 (Figure 7B).

To attempt to validate these *in silico* predictions, we evaluated experimentally the effect of three point mutations (^{65}L/S, ^{88}V/D and ^{98}V/S) in σ1A on the interaction with ClC-2ct by Y3H assays (Figure 7, C and D). We found that ^{65}L/S and ^{88}V/D mutations strongly abrogated the interaction.

Finally we examined whether we could detect any association *in vivo* between intact tetrameric AP-1 and ClC-2. MDCK cells stably expressing ClC-2-GFP were subjected to immunoprecipitation of detergent-solubilized membranes using an anti-γ adaptin antibody. Western blotting analysis revealed that the immunoprecipate contained ClC-2-GFP, indicating the existence of a complex between ClC-2-GFP and intact tetrameric AP-1.

DISCUSSION

A major incentive for these studies was the fact that, in spite of their growing relevance to a variety of physiological processes and human diseases, chloride channels remain vastly unexplored in terms of the mechanisms that control their subcellular distribution. We decided to focus on ClC-2 because of its physiological importance as a regulator of fluid transport in a variety of epithelia, including blood-retinal and blood-testis barriers (Bosl *et al.*, 2001; Nehrke *et al.*, 2002; Edwards *et al.*, 2010). Furthermore, ClC-2 provided an opportunity to study the sorting machinery involved in the trafficking of a basolateral protein with a dileucine sorting signal: although about a dozen proteins were shown to be sorted basolaterally in epithelial cells through dileucine motifs (Table 1), the molecules involved in their polarized distribution have not been characterized. A decade-old comparative study of normal and ClC-2 knock-out mice conclusively demonstrated the basolateral localization of this channel in intestinal mucosal epithelia and suggested that a dileucine motif in its cytoplasmic domain and the clathrin adaptor AP-1B were involved in its sorting (Peña-

Münzenmayer *et al.*, 2005). As ClC-2 has three dileucine motifs, we generated an *in silico* model of ClC-2 to assess their potential basolateral sorting role (Fig 1). Surprisingly, our model clearly indicated that TIFS^{812}LL, postulated to be the channel's basolateral sorting signal, was hidden in a dimerization region of the channel; thus, as dimerization likely occurs early during biogenesis (Jentsch, 2002), this motif would not be available to interact with the sorting machinery during trafficking to the cell surface. In contrast, ESMI^{623}LL and QVVA^{635}LL, the two other dileucine motifs, were exposed to the cytoplasm with ESMI^{623}LL having higher residue and side chain solvent accessibility than QVVA^{635}LL (Figure 1, Table 2), suggesting that one or both of them might perform as basolateral signals for ClC-2. These observations drove us to dissect the role of the three dileucine motifs in the basolateral sorting of ClC-2.

To initially characterize the possible sorting role of each dileucine motif, we carried out double alanine substitution of their leucine pairs (Figure 2). These studies confirmed the prediction of our *in silico* model regarding TIFS^{812}LL, as mutation of its dileucine pair did not disrupt the basolateral localization of HA-ClC-2. It is not clear why our results differ from those by Peña-Münzenmayer et al in this regard. Furthermore, our studies also clearly showed that double leucine replacement in either ESMI^{623}LL or QVVA^{635}LL in the context of the full-length channel caused strong intracellular retention of ClC-2 (Figure 2B, C). Furthermore, experiments with chimeras of the extracellular and transmembrane domains of p75 and the C-terminal domain of ClC-2 (p75-CLC-2ct) showed that wild type p75-CLC-2ct localized to the basolateral PM of MDCK cells whereas double leucine substitution of either ESMI^{623}LL or QVVA^{635}LL resulted in transport of the mutant proteins to the apical surface, rather than intracellular retention (Figure 5). The mislocalization of the mutant full size and chimeric channel reflect the absence of functional signals to promote trafficking from the sorting compartment to the cell surface. Whereas the retention of mutant ClC-2 reflects the lack of strong apical signals in its extracellular domain (just one N-glycan in the extracellular loop between the L and M α-helices (Figure 2A)), the apical localization of the mutant chimeric channel is driven by strong apical sorting signals, i.e. N- and O-glycans in the extracellular domain of p75 (Yeaman *et al.*, 1997). In agreement with this interpretation, it has been shown that disease causing mutations of a signal patch in the potassium channel Kir 2.1 required for binding AP-1 block export of the channel from the Golgi apparatus (Ma *et al.*, 2011). Taken together, these experiments suggested that ESMI^{623}LL and QVVA^{635}LL are required for the basolateral sorting of ClC-2 albeit not as independent and redundant basolateral signals. They also suggested that double alanine mutagenesis have insufficient resolution to distinguish between sorting and structural roles of each individual motif.

Both ESMI^{623}LL and QVVA^{635}LL are present within the highly structured CBS-1 domain of the cytoplasmic tail of ClC-2. Hence, in order to determine which one of these dileucine motifs behaves as a dileucine-based basolateral sorting signal, we used a classical and less intrusive strategy to study their sorting role, i.e. single alanine mutagenesis of all amino acid residues in each motif within the context of the full size channel. Strikingly, mutation of individual leucines in ESMI^{623}LL reduced basolateral localization and increased intracellular retention of the mutant channel whereas . mutagenesis of the -3, -2 and -1 (S, M and I) did not affect basolateral localization of the channel (Supplemental Figure S2). Mutagenesis of acidic residue ^{619}E did not cause

missorting of the channel, in agreement with the inconsistent sorting requirement for acidic residues in position -4 in dileucine motifs (Table 1) (Janvier *et al.*, 2003b; Mattera *et al.*, 2011) (Hunziker and Fumey, 1994) (Doumanov *et al.*, 2006). In contrast, replacement of each individual leucine in QVVA^{635}LL had no significant effect on the channel's distribution. These experiments strongly suggest that ESMI^{623}LL is the authentic basolateral sorting signal of ClC-2.

Because both variants of the clathrin adaptor AP-1, AP-1A and AP-1B, have been implicated in basolateral sorting, we then employed single or combined knock-down of AP-1A and AP-1B in MDCK cells, an approach we recently reported (Carvajal-Gonzalez et al., 2012; Gravotta et al., 2012), to study their role in basolateral sorting of ClC-2. Individual knock-down of either AP-1A or AP-1B did not disrupt the basolateral localization of ClC-2. In contrast, knock-down of both AP-1A and AP-1B resulted in intracellular retention of full length ClC-2 and in apical relocalization of the p75-ClC-2ct chimera (Figure 4, Figure 5). These results differ from gain of function experiments reported in AP-1B deficient LLC-PK1 cells showing that over- expression of the clathrin adaptor AP-1B but not of AP-1A corrects the non-polarized distribution of ClC-2. As AP-1A is expressed endogenously by LLC-PK1 cells, those experiments suggested that AP-1B but not AP-1A is necessary for basolateral expression of ClC-2 (Peña-Münzenmayer *et al.*, 2005). In contrast, our results demonstrate that expression of either AP-1A or AP-1B in MDCK cells is sufficient to confer basolateral localization to ClC-2.

If both AP-1A and AP-1B participate in the sorting of ClC-2, it should be possible to demonstrate that these adaptors interact specifically with this channel's basolateral sorting signal. Y3H studies have shown that [D/E]XXXL[L/I] dileucine motifs interact with γ–σ1, α–σ2 and δ–σ3 hemicomplexes in AP-1, AP-2 and AP-3, respectively; these interactions mediate the known biological functions of these adaptors, e.g., Nef-mediated down-regulation of CD4 and lysosomal targeting of LIMP-II. A recent study (Mattera *et al.*, 2011) has further shown that the interaction of dileucine motifs with AP-1 also depends on the combinatorial assembly of various γ □□□ σ1 isoforms, e.g. γ1 and γ2, and σ1A, σ1B and σ1C. For example, Nef and LIMP-II interacted with AP-1 hemicomplexes containing γ1 □□□ σ1A, B □□ C whereas tyrosinase interacted preferentially with γ2–σ1A □□□ γ2–σ1B hemicomplexes□□□Our studies demonstrated that the cytoplasmic domain of ClC-2 interacts well with γ1–σ1A, present in both AP-1A and AP-1B, as expected from our trafficking studies in MDCK cells silenced for both adaptors. This interaction was disrupted by alanine substitution ^{623}L/A but was unaffected by ^{635}L/A, strengthening the conclusion that ESMI^{623}LL controls the basolateral sorting of ClC-2 through direct interactions with the γ–σ□A hemicomplex present in both AP-1A and AP-1B. Furthermore, based on crystallographic and biochemical studies that have characterized the residues in the γ–σ1 and α–σ2 pockets that interact with the dileucine motifs (Janvier *et al.*, 2003b; Kelly *et al.*, 2008; Mattera *et al.*, 2011), we carried out *in silico* modeling experiments that suggested key interactions between ESMI^{623}LL and conserved residues in σ□A and confirmed these *in silico* predictions with Y3H assays.

In summary, our experiments characterize in detail the role of AP-1 in the sorting of a basolateral plasma membrane protein with a dileucine-based basolateral sorting signal in a model epithelial cell (MDCK). Although in this case AP-1A and AP-

1B appear to play equivalent roles in the sorting of ClC-2, other work in the field suggests that for certain basolateral proteins, particularly those with fast recycling kinetics, AP-1A cannot fully replace AP-1B (Gonzalez and Rodriguez-Boulan, 2009). Hence, current work in our laboratory aims to explore how exactly AP-1A mediates basolateral sorting in epithelial tissues that lack AP-1B, e.g. RPE (Diaz *et al.*, 2009) and kidney proximal tubule (Schreiner *et al.*, 2010). In addition, as there is significant evidence that ClC-2 may have an apical distribution in certain epithelial tissues, an important goal for the future is to study the possible role of ClC-2 interacting proteins such as GlialCAM and cereblon (Hohberger and Enz, 2009; Jeworutzki *et al.*, 2012), as potential accessory subunits of ClC-2 that regulate its trafficking in order to accommodate local tissue requirements. In addition, as ClC-2 displays a large intracellular pool and endocytic signals (Cornejo et al., 2009), it will be important in the future to study how post-endocytic recycling contributes to the surface polarity of this channel.

MATERIALS AND METHODS

Plasmids and mutagenesis

Vectors (pCR3.1) encoding ClC-2-GFP and HA-ClC-2 were kindly provided by Dr Francisco Sepulveda (Universidad de Valdivia, Chile) (Peña-Münzenmayer *et al.*, 2005). The p75-ClC-2ct chimera was constructed by amplification of C-terminus fragment of human ClC-2, corresponding to 347 residues (552-898) with forward and reverse primers containing BamHI and AscI restriction sites, respectively. The purified and digested ClC-2ct fragment was cloned into pCMV-75, designed to contain the complete extracellular and transmembrane domains and an 8-residue fragment of the cytoplasmic domain of p75 (Castorino et al., 2011). Single or double alanine substitution for leucines, as well as for other residues within ClC-2, ESMI^{623}LL, QVVA^{635}LL and TIFS^{812}LL motifs was performed using a QuikChange II site directed mutagenesis kit (Agilent Technologies). Custom-synthesized oligonucleotides were obtained from Fisher-Scientific (Thermo Fisher Scientific Inc.). All constructs were verified by sequencing.

RNA Interference

Silencing of μ1A and μ1B in MDCK cells was carried out by electroporation of the following siRNAs: μ1B (AACAAGCTGGTGACTGGCAAA) (Gravotta et al., 2007), μ1A (GTGCTCATCTGCCGGAATTTT) (Gravotta et al., 2012) or luciferase (GL2; Control), all synthesized by Dharmacon. Briefly, a suspension of $4x10^6$ of freshly trypsinized MDCK cells in 100 μl of Nucleofector solution V (Lonza Group Ltd), supplemented with 16 pmol of siRNA, was electroporated with the Nucleofector T-23 program (Lonza Group Ltd). This step was then repeated twice at three days intervals (Gravotta et al., 2012; Gravotta et al., 2007). RT-PCR and Western blot were used to confirm depletion of the targeted molecule.

Cell culture, transient expression and generation of permanent cell lines.

MDCK cells were maintained in growth media, DMEM (Cellgro) containing 5% Fetal Bovine Serum (FBS) at 37°C under 5% CO_2. Transient expression of HA-ClC-2 or p75-ClC-2ct chimeras in MDCK cells was carried out by electroporation-mediated transfection. Briefly, $2x10^6$ MDCK cells collected after trypsinization were suspended in 100 ul of Nucleofector solution V (Lonza Group Ltd) containing 5µg of either pCR3.1(HA-ClC-2) or pCMV(75-ClC-2ct) and electroporated with the Nucleofector T-23 program (Lonza Group Ltd). Permanent MDCK cell lines expressing either HA-ClC-2 or p75-ClC-2ct were generated by transfecting MDCK cells with Lipofectamine 2000, following manufacturer recommendations (Life Technologies, Grand Island, NY). Cells expressing the desired proteins were selected in growth media supplemented with 0.8mg/ml G418 and isolated with cloning rings.

Immunolabeling and quantification.

Immunolabeling of transiently transfected MDCK cells or permanent MDCK cell lines obtained as described above, was carried out on 12mm Transwell chambers with 0.4 µm polycarbonate membranes (Costar) seeded with 300,000 cells/cm^2 and processed 3.5-4 days after full polarization. Cell surface expression of HA-ClC-2 or chimeras of p75-ClC-2ct was determined by sequential immunolabeling using two different species of antibodies. Cells were rinsed twice at 37ºC and once at 4ºC with HBSS containing Ca^{++} and Mg^{++} (HBSS-CaMg) and then incubated at 4ºC for 30 min. with HBSS-CaMg containing 1.5% BSA followed by the addition of either rat monoclonal antibody against HA or mouse monoclonal antibody against p75 (1/100) and further incubated at 4^oC for 4h to label surface exposed luminal HA-epitope in cells expressing HA-ClC-2 or luminal p75 epitopes in cells expressing p75-ClC-2ct chimera (channel 1, intact cells). Cells were rinsed 4 times with HBSS-CaMg-1.5% BSA and fixed with 3.7% paraformaldehyde (PFA) for 20 minutes at 4ºC, rinsed and the aldehyde excess quenched with 50 mM NH_4Cl in PBS for 20min at room temperature (RT). Total, intracellular and surface expression was detected after cell permeabilization with 0.075% saponin in PBS at RT for 10 min., followed by a 30 min. wash at RT with HBSS-CaMg-1.5% BSA and overnight incubation at 4ºC with mouse monoclonal anibody against HA or rabbit polyclonal antibody against p75, respectively (channel 2, permeabilized cells). Excess antibody was eliminated by 4 rinses with HBSS-CaMg-1.5% BSA. Primary antibodies bound during these sequential incubations were visualized with secondary goat antibodies labeled with Alexa-Fluor®488 568 or 647 (Life Technologies), as indicated. Cells were then rinsed 4 times with HBSS-CaMg-1.5% BSA and mounted in Vectashield™. Samples were examined with a Zeiss spinning disc confocal microscope, equipped with a Yokogawa scanner unit and Zeiss Plan apochromat 63X/1.46-0.60 oil-immersion objective. Confocal image stacks were acquired at 512 x 512 with high sensistivity Hamamatsu Evolve™ EMCCD cameras (Photometrics; Tucson, Arizona). The acquired image stacks of 90-120 slices (z = 1 to n=90–120) were processed to generate region of interest (ROI) containing average of 2 cells per ROI. The fluorescence images associated with ch2 (labeling all cargoes in permeabilized cells) and ch1 (labeling surface cargoes on intact cells at 4ºC) within

these ROI were analyzed with Zen imaging software (Zeiss, Oberkochen, Germany) to generate the following data files:

${}^{col}_{1}Px$ (surface): pixels within ch2 (permeabilized cells) that <u>colocalize</u> with ch1.(intact cells).
${}^{col}_{ch2}Mi$: mean intensity of the above colocalizing pixels in ch2.

${}^{1}_{ch2}Px$ (intracellular): pixels within ch2 (permeabilized cells) that <u>do not colocalize</u> with ch1 (intact cells).
${}^{1}_{ch2}Mi$: mean intensity of the above non-colocalizing pixels within ch2.

The equation described below is an operator that sums i the product of pixel (Px) number and the mean intensity (Mi) within an ROI for all z =1-n slices of each image stack.

Surface total (S_t) (colocalized)
$S_t = \sum_{z=1}^{n} [\ {}^{col}_{1}Px\ x\ {}^{col}_{ch2}Mi\ ]$

Intracellular total (IC_t) (not-colocalized)
$IC_t = \sum_{z=1}^{n} [\ {}^{1}_{ch2}Px\ x\ {}^{1}_{ch2}Mi\ ]$

The values obtained represent total surface (S_t) and total intracellular (IC_t) cargoes. The fraction of total cargo on the surface vs intracellular pools, represented in the bar graphs of figure 3, 4, 5 and Supplemental Figure S2 is calculated as follows.

Surface (fraction of total) = S_t / S_t + IC_t

Intracellular (fraction of total) = IC_t / S_t + IC_t

Statistical analyses.
Data derived from images collected and processed as described above were analyzed by one-way ANOVA to obtained mean, standard deviation and probability (p) values. The p values obtained were subjected to multiple hypothesis testing using Bonferroni's corrections. All analyses were performed with statistical software Origin9.1 (OriginLab Corp, Northampton, MA).

Molecular modeling of ClC-2 and the interactions of its ESMI^{623}LL motif with AP-1.
The comparative modeling of human ClC-2 was performed using the MODELLER program (Webb and Sali, 2014) as implemented in the Build Homology Model module of Discovery Studio v2.1 software (Accelrys Inc., San Diego, USA). We used a suitable template for modeling ClC-2 (Uniprot, P51788) the crystal structure of Cyanidioschyzon merolae eukaryotic ClC transporter (CmClC) (PDB 3ORG, at 3.5Å resolution (Feng *et al.*, 2010).The missing extracellular loop residues were constructed

using bacterial ClCs (PDB IDs 1OTS, 1KPL) (Dutzler *et al.*, 2002, 2003). The CBS domains of ClC-2 were modeled using the reported structures of cytoplasmic domains of ClC-Ka (PDB 2PFI) (Markovic and Dutzler, 2007b) and ClC-0 (PDB 2D4Z). Using the previously completed CmClC structure, the sequence alignment considered secondary structure predictions and PFAM sequence conservation for domains CLC (PF00654) and CBS (PF00571). For modeling purposes the first 83 residues and those corresponding to segments 663-694 and 725-771 were not included due to lack of an appropriate template. The protein was modeled as a dimer, and 100 models were generated, the best model ranked by Modeller (internal PDF score) was energy minimized using the conjugate gradient algorithm until a RMS gradient of 0,001 kcal/molÅ was reached. The CHARMM22 force field with a dielectric constant of 4 and a distance-dependent dielectric implicit solvent model to mimic the membrane environment was employed (Brooks *et al.*, 2009). Model quality assessment was performed using the SAVES server (http://nihserver.mbi.ucla.edu/SAVES/), which indicates that the obtained model has more than 95% of residues in the allowed regions according to Ramachandran plot analysis.

We modeled the active AP-1A complex interacting with the canonical dileucine motif present in CD4 co-crystallized with AP2 (PDB id 2JKR) (Kelly *et al.*, 2008; Jackson *et al.*, 2010). Accordingly we propose that AP-1A may interact with the dileucine motif ESMI^{623}LL of CBS1. Thus, we modeled the interaction between the dileucine binding pocket in the γ1−σ1A heterocomplex of AP-1 with a ClC-2 617-621 peptide containing the ESMI^{623}LL dileucine motif (SPESMI^{623}LLG). The obtained complex was relaxed using molecular mechanics minimization using the CHARMM22 force field in Discovery Studio v2.1, using the conjugate gradient algorithm with a distance-dependent dielectric implicit solvent model with a dielectric constant of 80, until a RMS gradient of 0.0001 kcal/molÅ was reached.

Yeast three-hybrid assays (Y3H).

The C-cytoplasmic domain of ClC-2 was amplified and cloned into the multiple cloning site 1 (MCS-1) of pBridge vector (Clontech; Mountain view, CA) using EcoRI and SalI restriction sites. A cDNA encoding σ1A subunit was cloned into the MCS-2 (GAL4-BD) of pBridge using the NotI and BglII restriction sites. The constructs containing β1 subunit (GAL4-AD-β) or γ1 subunit (GAL4-AD-γ) were a gift from Dr. Bonifacino (Janvier *et al.*, 2003b). Alanine substitution of selected residues within σ1A, ^{65}L/S, ^{88}V/D, ^{98}V/S, were performed using a QuikChange II site directed mutagenesis kit (Agilent Technologies) with custom-synthesized oligonucleotides from Fisher-Scientific (Thermo Fisher Scientific Inc.). Yeast three-hybrid assays were carried out with strain HF7c (Clontech; Mountain view, CA) as reported previously (Janvier *et al.*, 2003b) using a lithium acetate transformation protocol (Clontech; Mountain view, CA). Transformed HF7c cells were selected in medium lacking leucine, tryptophan and methionine (DOB-3). Bait-pray interaction was determined by spotting transformed cells from diluted samples (0.05 OD^{600}) on plates lacking tryptophan, leucine, methionine and histidine (DOB-4) after 4-6 days incubation at 30°C. Plates were recorded with a scanner (EPSON model 3200). Quantitative assays

were carried out by growing transformed cells in liquid media (DOB-4) by duplicate for 5-6 days monitoring O.D.^{600} at indicated intervals.

Lentivirus generation and cell transduction.

Wild type and mutant forms of CLC2-HA were subcloned in the pCCL-PGK lentiviral vector (kindly provided by Dr. Shahin Rafii, Weill Cornell Medical College), and lentiviruses were generated as previously described (Seandel *et al.*, 2008). Viral supernatants were concentrated 100 fold with the Lenti-X Concentrator (Clontech Laboratories, Inc.) following the manufacturer's instructions. For viral titration, total RNA was isolated from the concentrated viral preparations with the RNeasy Mini Kit (Qiagen), including an in-column DNAse digestion step. Viral RNA was converted to cDNA with the High Capacity cDNA Reverse Transcription Kit (Life Technologies) and quantified in a StepOnePlus Real-Time PCR System (Life Technologies) using SYBR Select Master Mix (Life Technologies) and HIV RRE-specific primers (5'-GTATAGTGCAGCAGCAGAAC-3' and 5'-ACAGCAGTGGTGCAAATGAG-3'). Quantification was performed by interpolation into a standard curve.

For cell transduction, 1.5×10^5 MDCK cells were seeded on 12mm Transwell chambers with 0.4 µm pore polycarbonate membranes (Costar). After 24h, 50 viral genome equivalents/cell were added to the top chamber in the presence of 6 µg/ml polybrene (Sigma), and the inoculum was replaced by fresh media 24h later. Three days later, fully polarized cells were processed for further analysis.

Domain-selective biotinylation and surface biotin avidin shift (SBAS) assay.

Cell surface biotinylation and surface biotinylated avidin shift (SBAS) assays were carried out as previously described (Gravotta et al., 2012). This assay, differently from the conventional surface domain biotinylation-streptavidin retrieval assay (REF), quantifies the steady state apical/basolateral surface distribution of a given protein as a fraction of the total protein pool. Briefly, fully polarized MDCK monolayers seeded at 300,000 cells.cm^{-2} on 0.4 µm polycarbonate membranes in 12 mm Transwell chambers were subjected to domain selective biotinylation using sulpho-NHS-LC-biotin, twice for 20 min at 4°C, either apically or basolaterally. Identical (60µl) aliquots of a lysate made in Tris-HCl 40mM pH 7.8. 5mM EDTA, 1% SDS containing a protease inhibitor cocktail were supplemented with 25mM DTT and heated at 65ºC for 10min, mixed with 55µl of a buffer containing 500µg/ml avidin, 35% glycerol and 15µg/ml bromophenol blue, supplemented with 1.2mM biotin (biotin +) or not (biotin -) and heated at 65ºC for 10min (Gravotta et al., 2012). Samples were resolved side by side by SDS PAGE, processed for western blot with antibodies against cargo proteins and quantified using ECL (GE Healthcare) or Odyssey (Licor^{R}-Bioscience).
Under the conditions of this assay, the intensity differences between the electrophoretic gel bands in biotin + and biotin - samples represent the pool of biotinylated cargo molecules localized at apical (AP) and basolateral (BL) domains, as a fraction of the total cargo pool (Gravotta *et al.*, 2012), as follows:

For apically biotinylated cells: AP-cargo = [(biotin +) – (biotin -)] / (biotin +)

For basolaterally biotinylated cells: BL-cargo = [(biotin +) – (biotin -)] / (biotin +)

Intracellular cargo is calculated as IC-cargo = 1- (AP-cargo – BL-cargo)

Immunoprecipitation

MDCK cells expressing GFP-ClC-2 were lysed at 4°C with lysis buffer (1% Triton X-100, 25mM Tris-Cl pH 7.5, 150mM NaCl, 0.5mM EDTA, 10% Glycerol) and a cocktail of protease inhibitors. The lysate was pre-cleared by centrifugation at 10,000 rpm for 15min and the supernatant incubated with 1.5µg of mouse anti-gamma adaptin antibody absorbed to 50µl of dynabeads (Life Technologies; Carlsbad, CA) for 3 hours at 4ºC. The immuno-complexes were washed 5 times with lysis buffer, once with wash buffer in dynabead kit and eluted with Laemmli sample buffer 3.6X. The samples were heated at 70°C for 10min, resolved by 4-12% SDS-PAGE and processed for western blot with either primary mouse anti-gamma adaptin or chicken anti-GFP antibodies followed by secondary antibodies labeled with red IRDye^{680} (anti-mouse) and green IRDye^{800} (anti-chicken) and imaged using Odyssey (Licor^{R}-Bioscience)

ACKNOWLEDGEMENTS

This work was supported by NIH grants GM34107 and EY08531 to ERB, by a Beca-Chile fellowship to EF-O, by a Pew Latin American Fellowship to GL and by the Dyson Foundation and the Research to Prevent Blindness Foundation.

REFERENCES

Blaisdell, C. J., Edmonds, R. D., Wang, X. T., Guggino, S., and Zeitlin, P. L. (2000). pH-regulated chloride secretion in fetal lung epithelia. Am. J. Physiol. Lung Cell. Mol. Physiol. *278*, L1248–L1255.

Bonifacino, J. S. (2014). Adaptor proteins involved in polarized sorting. J. Cell Biol. *204*, 7–17.

Bonifacino, J. S., and Traub, L. M. (2003). Signals for sorting of transmembrane proteins to endosomes and lysosomes. Annu Rev Biochem *72*, 395–447.

Bosl, M. R., Stein, V., Hubner, C., Zdebik, A. A., Jordt, S. E., Mukhopadhyay, A. K., Davidoff, M. S., Holstein, A. F., and Jentsch, T. J. (2001). Male germ cells and photoreceptors, both dependent on close cell-cell interactions, degenerate upon ClC-2 Cl(-) channel disruption. EMBO J *20*, 1289–1299.

Brooks, B. R. *et al.* (2009). CHARMM : The Biomolecular Simulation Program.

Carvajal-Gonzalez, J. M., Gravotta, D., Mattera, R., Diaz, F., Perez Bay, A., Roman, A. C., Schreiner, R. P., Thuenauer, R., Bonifacino, J. S., and Rodriguez-Boulan, E. (2012). Basolateral sorting of the coxsackie and adenovirus receptor through interaction of a canonical YXXPhi motif with the clathrin adaptors AP-1A and AP-1B. Proc Natl Acad Sci U S A *109*, 3820–3825.

Castorino, J. J., Deborde, S., Deora, A., Schreiner, R., Gallagher-Colombo, S. M., Rodriguez-Boulan, E., and Philp, N. J. (2011). Basolateral sorting signals regulating tissue-specific polarity of heteromeric monocarboxylate transporters in epithelia. Traffic *12*, 483–498.

Catalán, M., Niemeyer, M. I., Cid, L. P., and Sepúlveda, F. V. (2004). Basolateral ClC-2 chloride channels in surface colon epithelium: regulation by a direct effect of intracellular chloride☆. Gastroenterology *126*, 1104–1114.

Catalan, Marcelo, Cornejo, I., Figueroa, C. D., Niemeyer, I., and Sepu, F. V (2002). ClC-2 in guinea pig colon : mRNA , immunolabeling , and functional evidence for surface epithelium localization. 1004–1013.

Cornejo, I., Niemeyer, M. I., Zuniga, L., Yusef, Y. R., Sepulveda, F. V, and Cid, L. P. (2009). Rapid recycling of ClC-2 chloride channels between plasma membrane and endosomes: role of a tyrosine endocytosis motif in surface retrieval. J Cell Physiol *221*, 650–657.

Deborde, S., Perret, E., Gravotta, D., Deora, A., Salvarezza, S., Schreiner, R., and Rodriguez-Boulan, E. (2008). Clathrin is a key regulator of basolateral polarity. Nature *452*, 719–723.

Diaz, F., Gravotta, D., Deora, A., Schreiner, R., Schoggins, J., Falck-Pedersen, E., and Rodriguez-Boulan, E. (2009). Clathrin adaptor AP1B controls adenovirus infectivity of epithelial cells. Proc. Natl. Acad. Sci. U. S. A. *106*, 11143–11148.

Doray, B., Lee, I., Knisely, J., Bu, G., and Kornfeld, S. (2007). The gamma/sigma1 and alpha/sigma2 hemicomplexes of clathrin adaptors AP-1 and AP-2 harbor the dileucine recognition site. Mol Biol Cell *18*, 1887–1896.

Doumanov, J. A., Daubrawa, M., Unden, H., and Graeve, L. (2006). Identification of a basolateral sorting signal within the cytoplasmic domain of the interleukin-6 signal transducer gp130. Cell. Signal. *18*, 1140–1146.

Dutzler, R., Campbell, E. B., Cadene, M., Chait, B. T., and MacKinnon, R. (2002). X-ray structure of a ClC chloride channel at 3.0 A reveals the molecular basis of anion selectivity. Nature *415*, 287–294.

Dutzler, R., Campbell, E. B., and MacKinnon, R. (2003). Gating the selectivity filter in ClC chloride channels. Science *300*, 108–112.

Edwards, M. M. *et al.* (2010). Photoreceptor degeneration, azoospermia, leukoencephalopathy, and abnormal RPE cell function in mice expressing an early stop mutation in CLCN2. Invest Ophthalmol Vis Sci *51*, 3264–3272.

Feng, L., Campbell, E. B., Hsiung, Y., and MacKinnon, R. (2010). Structure of a eukaryotic CLC transporter defines an intermediate state in the transport cycle. Science (80-.). *330*, 635–641.

Fölsch, H., Ohno, H., Bonifacino, J. S., and Mellman, I. (1999). A novel clathrin adaptor complex mediates basolateral targeting in polarized epithelial cells. Cell *99*, 189–198.

Le Gall, A. H., Powell, S. K., Yeaman, C. A., and Rodriguez-Boulan, E. (1997). The neural cell adhesion molecule expresses a tyrosine-independent basolateral sorting signal. J. Biol. Chem. *272*, 4559–4567.

Gan, Y., McGraw, T. E., and Rodriguez-Boulan, E. (2002). The epithelial-specific adaptor AP1B mediates post-endocytic recycling to the basolateral membrane. Nat. Cell Biol. *4*, 605–609.

Garcia-Olivares, J., Alekov, A., Boroumand, M. R., Begemann, B., Hidalgo, P., and Fahlke, C. (2008). Gating of human ClC-2 chloride channels and regulation by carboxy-terminal domains. J Physiol *586*, 5325–5336.

Gonzalez, A., and Rodriguez-Boulan, E. (2009). Clathrin and AP1B: key roles in basolateral trafficking through trans-endosomal routes. FEBS Lett. *583*, 3784–3795.

Gravotta, D., Carvajal-Gonzalez, J. M., Mattera, R., Deborde, S., Banfelder, J. R., Bonifacino, J. S., and Rodriguez-Boulan, E. (2012). The clathrin adaptor AP-1A mediates basolateral polarity. Dev. Cell *22*, 811–823.

Gravotta, D., Deora, A., Perret, E., Oyanadel, C., Soza, A., Schreiner, R., Gonzalez, A., and Rodriguez-Boulan, E. (2007). AP1B sorts basolateral proteins in recycling and biosynthetic routes of MDCK cells. Proc. Natl. Acad. Sci. U. S. A. *104*, 1564–1569.

Gründer, S., Thiemann, A., Pusch, M., and Jentsch, T. J. (1992). Regions involved in the opening of CIC-2 chloride channel by voltage and cell volume. Nature *360*, 759–762.

Gyömörey, K., Yeger, H., Ackerley, C., Garami, E., and Bear, C. E. (2000). Expression of the chloride channel ClC-2 in the murine small intestine epithelium. Am. J. Physiol. Cell Physiol. *279*, C1787–C1794.

Hohberger, B., and Enz, R. (2009). Cereblon is expressed in the retina and binds to voltage-gated chloride channels. FEBS Lett. *583*, 633–637.

Hunziker, W., and Fumey, C. (1994). A di-leucine motif mediates endocytosis and basolateral sorting of macrophage IgG Fc receptors in MDCK cells. EMBO J. *13*, 2963–2969.

Jackson, L. P., Kelly, B. T., McCoy, A. J., Gaffry, T., James, L. C., Collins, B. M., Höning, S., Evans, P. R., and Owen, D. J. (2010). A large-scale conformational change couples membrane recruitment to cargo binding in the AP2 clathrin adaptor complex. Cell *141*, 1220–1229.

Janvier, K., Kato, Y., Boehm, M., Rose, J. R., Martina, J. A., Kim, B. Y., Venkatesan, S., and Bonifacino, J. S. (2003a). Recognition of dileucine-based sorting signals from HIV-1 Nef and LIMP-II by the AP-1 gamma-sigma1 and AP-3 delta-sigma3 hemicomplexes. J Cell Biol *163*, 1281–1290.

Janvier, K., Kato, Y., Boehm, M., Rose, J. R., Martina, J. A., Kim, B.-Y., Venkatesan, S., and Bonifacino, J. S. (2003b). Recognition of dileucine-based sorting signals from HIV-1 Nef and LIMP-II by the AP-1 gamma-sigma1 and AP-3 delta-sigma3 hemicomplexes. J. Cell Biol. *163*, 1281–1290.

Jentsch, T. . J. (2005). Chloride transport in the kidney: lessons from human disease and knockout mice. J Am Soc Nephrol *16*, 1549–1561.

Jentsch, T. J. (2002). Chloride channels are different. Nature *415*, 276–277.

Jentsch, T. J. (2008). CLC chloride channels and transporters: from genes to protein structure, pathology and physiology. Crit Rev Biochem Mol Biol *43*, 3–36.

Jentsch, T. J., Maritzen, T., and Zdebik, A. A. (2005). Review series Chloride channel diseases resulting from impaired transepithelial transport or vesicular function. *115*.

Jeworutzki, E. *et al.* (2012). GlialCAM, a protein defective in a leukodystrophy, serves as a ClC-2 Cl(-) channel auxiliary subunit. Neuron *73*, 951–961.

Johnson, K. F., and Kornfeld, S. (1992). The cytoplasmic tail of the mannose 6-phosphate/insulin-like growth factor-II receptor has two signals for lysosomal enzyme sorting in the Golgi. J. Cell Biol. *119*, 249–257.

Kelly, B. T., McCoy, A. J., Spate, K., Miller, S. E., Evans, P. R., Honing, S., and Owen, D. J. (2008). A structural explanation for the binding of endocytic dileucine motifs by the AP2 complex. Nature *456*, 976–979.

Letourneur, F., and Klausner, R. D. (1992). A novel di-leucine motif and a tyrosine-based motif independently mediate lysosomal targeting and endocytosis of CD3 chains. Cell *69*, 1143–1157.

Lipecka, J., Bali, Z., Thomas, A., Fanen, P., Edelman, A., Fritsch, J., and Distri-, J. F. (2002). Distribution of ClC-2 chloride channel in rat and human epithelial tissues. 805–816.

Ma, D., Taneja, T. K., Hagen, B. M., Kim, B. Y., Ortega, B., Lederer, W. J., and Welling, P. A. (2011). Golgi export of the Kir2.1 channel is driven by a trafficking signal located within its tertiary structure. Cell *145*, 1102–1115.

Markovic, S., and Dutzler, R. (2007a). The structure of the cytoplasmic domain of the chloride channel ClC-Ka reveals a conserved interaction interface. Structure *15*, 715–725.

Markovic, S., and Dutzler, R. (2007b). The structure of the cytoplasmic domain of the chloride channel ClC-Ka reveals a conserved interaction interface. Structure *15*, 715–725.

Mattera, R., Boehm, M., Chaudhuri, R., Prabhu, Y., and Bonifacino, J. S. (2011). Conservation and diversification of dileucine signal recognition by adaptor protein (AP) complex variants. J Biol Chem *286*, 2022–2030.

Murray, C. B., Morales, M. M., Flotte, T. R., McGrath-Morrow, S. A., Guggino, W. B., and Zeitlin, P. L. (1995). CIC-2: a developmentally dependent chloride channel expressed in the fetal lung and downregulated after birth. Am. J. Respir. Cell Mol. Biol. *12*, 597–604.

Nakatsu, F., Hase, K., and Ohno, H. (2014). The Role of the Clathrin Adaptor AP-1: Polarized Sorting and Beyond. Membranes (Basel). *4*, 747–763.

Nehrke, K., Arreola, J., Nguyen, H.-V., Pilato, J., Richardson, L., Okunade, G., Baggs, R., Shull, G. E., and Melvin, J. E. (2002). Loss of hyperpolarization-activated Cl(-) current in salivary acinar cells from Clcn2 knockout mice. J. Biol. Chem. *277*, 23604–23611.

Ohno, H., Tomemori, T., Nakatsu, F., Okazaki, Y., Aguilar, R. C., Foelsch, H., Mellman, I., Saito, T., Shirasawa, T., and Bonifacino, J. S. (1999). Mu1B, a novel adaptor medium chain expressed in polarized epithelial cells. FEBS Lett. *449*, 215–220.

Peña-Münzenmayer, G., Catalán, M., Cornejo, I., Figueroa, C. D., Melvin, J. E., Niemeyer, M. I., Cid, L. P., and Sepúlveda, F. V (2005). Basolateral localization of native ClC-2 chloride channels in absorptive intestinal epithelial cells and basolateral sorting encoded by a CBS-2 domain di-leucine motif. J. Cell Sci. *118*, 4243–4252.

Puertollano, R., Aguilar, R. C., Gorshkova, I., Crouch, R. J., and Bonifacino, J. S. (2001). Sorting of mannose 6-phosphate receptors mediated by the GGAs. Science (80-.). *292*, 1712–1716.

Schreiner, R., Frindt, G., Diaz, F., Carvajal-Gonzalez, J. M., Perez Bay, A. E., Palmer, L. G., Marshansky, V., Brown, D., Philp, N. J., and Rodriguez-Boulan, E. (2010). The absence of a clathrin adapter confers unique polarity essential to proximal tubule function. Kidney Int. *78*, 382–388.

Seandel, M. *et al.* (2008). Generation of a functional and durable vascular niche by the adenoviral E4ORF1 gene. Proc. Natl. Acad. Sci. U. S. A. *105*, 19288–19293.

Stauber, T., and Jentsch, T. J. (2010). Sorting motifs of the endosomal/lysosomal CLC chloride transporters. J Biol Chem *285*, 34537–34548.

Stölting, G., Fischer, M., and Fahlke, C. (2014). CLC channel function and dysfunction in health and disease. Front. Physiol. *5*, 378.

Strange, K. (2011). Putting the pieces together: A crystal clear window into CLC anion channel regulation. Channels *5*, 101–105.

Strauss, O. (2005). The retinal pigment epithelium in visual function. Physiol Rev *85*, 845–881.

Thiemann, A., Gründer, S., Pusch, M., and Jentsch, T. J. (1992). A chloride channel widely expressed in epithelial and non-epithelial cells. Nature *356*, 57–60.

Traub, L. M. (2009). Tickets to ride: selecting cargo for clathrin-regulated internalization. Nat. Rev. Mol. Cell Biol. *10*, 583–596.

Webb, B., and Sali, A. (2014). Comparative Protein Structure Modeling Using MODELLER.

Yeaman, C., Le Gall, A. H., Baldwin, A. N., Monlauzeur, L., Le Bivic, A., and Rodriguez-Boulan, E. (1997). The O-glycosylated stalk domain is required for apical sorting of neurotrophin receptors in polarized MDCK cells. J. Cell Biol. *139*, 929–940.

Zhu, Y., Doray, B., Poussu, A., Lehto, V. P., and Kornfeld, S. (2001). Binding of GGA2 to the lysosomal enzyme sorting motif of the mannose 6- phosphate receptor. Science (80-.). *292*, 1716–1718.

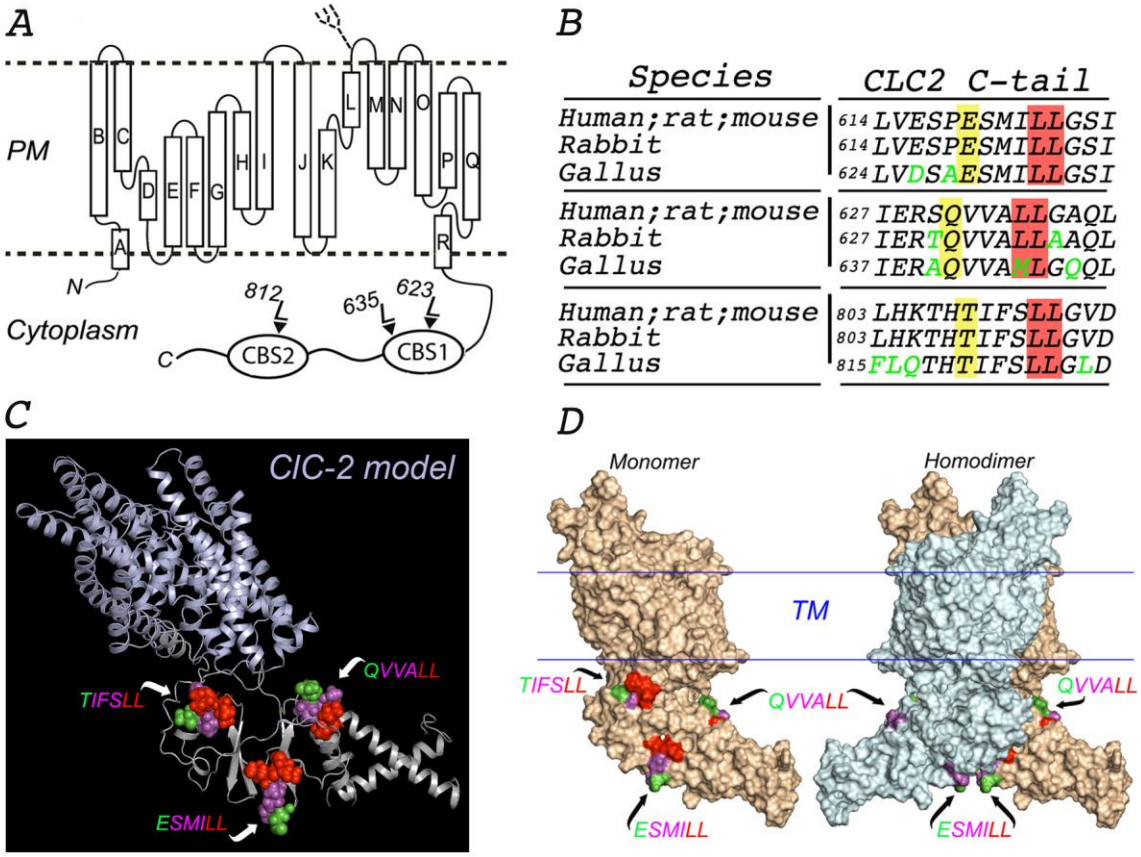

Figure 1. In silico molecular model of ClC-2.

A) Proposed topology of human ClC-2. ClC-2 displays 18 alpha helices (A-R) that span the membrane, both N- and C-terminus ends facing the cytoplasm. The C-terminus of ClC-2 contains the CBS1 and CBS2 domains, which display two and one dileucine motifs, respectively. A single N-linked glycan is present on the short luminal loop between the L and M alpha helices, as indicated.

B) Multiple sequence alignment using Clustal Omega program (UniProt) with sequences from the indicated species (P51788, human; P35525, rat; Q9R0A1, mouse; P51789, rabbit; XP 423073.4, gallus). The amino acid sequences around each of the three dileucine motifs in the cytoplasmic tail of ClC-2 are conserved in mammals (human, rat, mouse and rabbit). One of the two leucines in the QVVA^{645}LL motif is changed to a methione (QVVA^{645}ML) in birds (gallus). Conserved residues are shown in black whereas non-conserved residues are shown in green. The critical leucine pair and residues at position -4 are shaded in red and yellow, respectively.

C) Combined cartoon rendered structure in a monomer of ClC-2 displaying the three dileucine motifs in a sphere format. We modeled the structure of ClC-2 (UniProt P51788) using MODELLER and available crystal structure information for the

transmembrane and extracellular domains of CmClC (3ORG), EcClC (1OTS) and StCLC (1KPL) and for the CBS domains of ClC-Ka (2PFI) and ClC-0 (2D4Z).

D) Surface-rendered structure of ClC-2 monomer (left) and homodimer (right) displaying the three dileucine motifs. TIFS ^{812}LL is present in a region of CBS2 that participates in the dimerization of the channel and is thus hidden in the dimer. For each motif, essential L residues are represented in red, non essential variable residues at -1, -2, -3 positions are displayed in magenta and the residues at -4 position in shown in green.

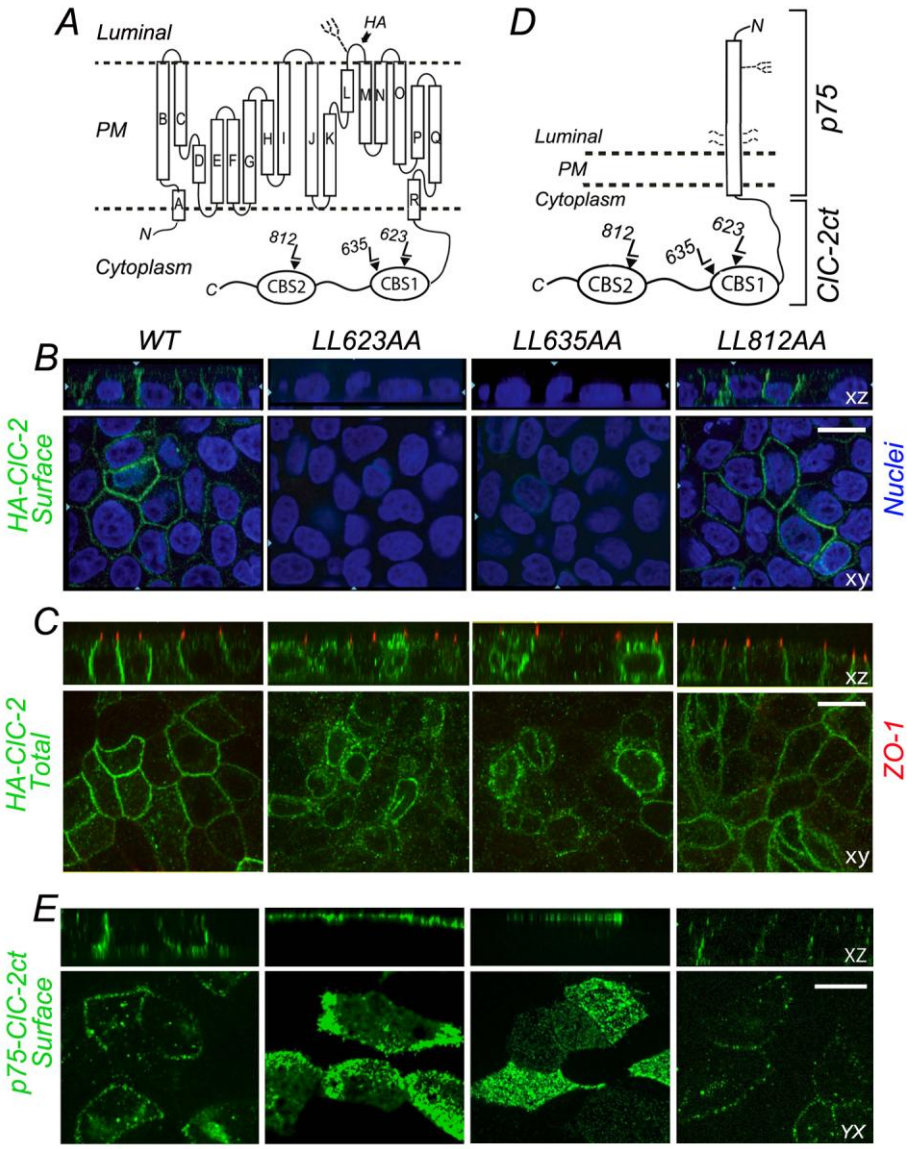

Figure 2. Basolateral localization of ClC-2 is disrupted by L->A mutagenesis of ESMI^{623}LL or QVVA^{635}LL

A) Cartoon representation of HA-tagged ClC-2. The HA epitope is located in the short luminal loop between L and M alpha helices; this loop contains an N-linked glycan. Note the CBS1 and CBS2 domains in the C-terminus that house the three dileucine motifs.

B) Stable MDCK cell lines expressing wild type (WT) or mutant HA-ClC-2 with alanine replacements of dileucine pairs for each individual dileucine motif, HA-ClC-2[^{623}LL/AA], HA-ClC-2[^{635}LL/AA] and HA-ClC-2[^{812}LL/AA]. Cells were polarized after 4 days in cultured on Transwell filters and immunolabeled with HA antibody before permeabilization to decorate surface ClC-2 (green). Note the basolateral

localization of HA-ClC-2[WT] and HA-ClC-2[^{812}LL/AA]; in contrast, HA-ClC-2[^{623}LL/AA] and HA-ClC-2[^{635}LL/AA] are not expressed at the cell surface

C) The same cell lines shown in B were decorated with HA antibodies after cell permeabilization; tight junctions are labeled with anti-ZO1 (red). Note the intracellular accumulation of HA-ClC-2[^{623}LL/AA] and HA-ClC-2[^{635}LL/AA] mutants.

D) Cartoon representation of p75-ClC-2ct chimera constructed by fusing the luminal, transmembrane and 8 cytoplasmic residues of p75 with the entire C-terminus domain (347 aa) of ClC-2. The single N-linked glycan and four O-linked glycans of p75 are displayed.

E) Stable MDCK cells lines expressing wild type p75-ClC-2ct or the dileucine mutants p75-ClC-2ct[^{623}LL/AA], p75-ClC-2ct[^{635}LL/AA] and p75-ClC-2ct[^{812}LL/AA]. Cells were cultured for 4 days on Transwell filters, fixed without permeabilization and immunolabeled with mouse antibodies to the ectodomain of p75 (green) to visualize the surface distribution of the chimeric proteins. Note the basolateral localization of WT p75-ClC-2ct and p75-ClC-2ct[^{812}LL/AA] and the apical redistribution of p75-ClC-2ct[^{623}LL/AA] and p75-ClC-2ct[^{635}LL/AA] .

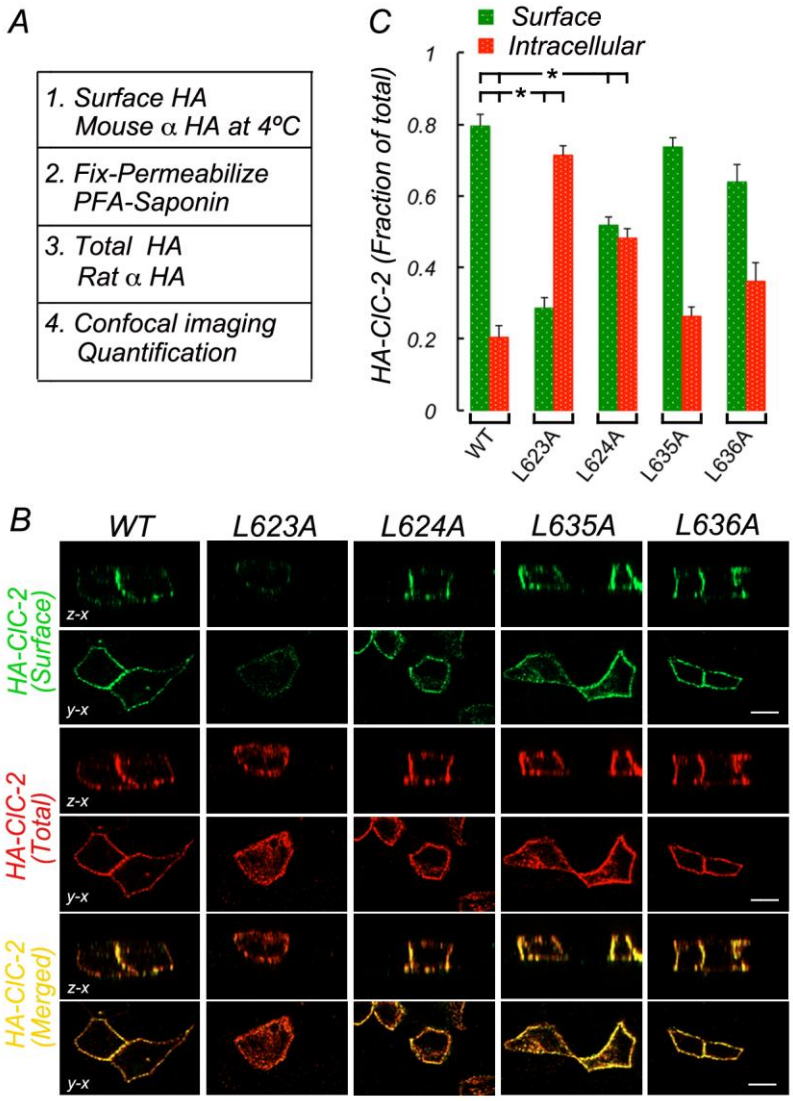

Figure 3. ESMI^{623}LL motif controls basolateral localization of HA-ClC-2.
Wild type and mutant HA-CLC-2 with single leucine residues replaced by alanine in ESMI^{623}LL or QVVA^{635}LL were transiently expressed in MDCK cells allowed to polarize for 4 days in culture.
A) Procedure to sequentially immunolabel HA-ClC-2 before and after saponin permeabilization with mouse and rat antibodies to luminal HA, respectively (See Materials and Methods for details).
B) Surface (green) and total (red) HA-ClC-2 in fully polarized cells. Note that wild type HA-ClC-2[WT] is restricted to the basolateral membrane whereas HA-ClC-2 [^{623}L/A] is depleted from the cell surface and accumulated intracellularly.

C) Bars represent fractions of surface and intracellular HA-ClC-2 calculated from confocal images , (see Materials and Methods for details). Statistically significant

reductions in surface localization of HA-ClC-2 [^{623}L/A] and HA-ClC-2 [^{624}L/A] are indicated. No significant changes in HA-ClC-2 [^{635}L/A] or HA-ClC-2 [^{636}L/A].were observed. Detailed statistical analysis is shown in supplemental Table S1. Bar= 12 μm.

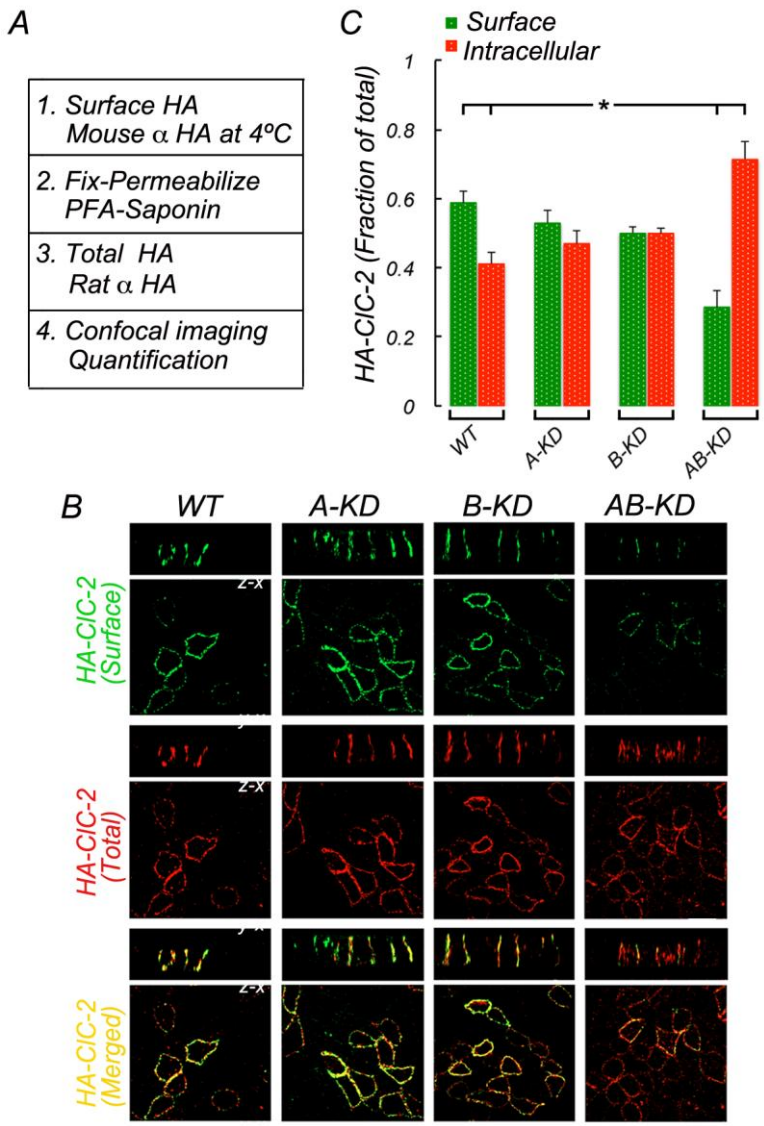

Figure 4. Double knock-down of clathrin adaptors AP-1A and AP-1B inhibits surface expression of full length ClC-2.

MDCK cells, wild type (WT) or depleted of μ1A (A-KD), μ1B (B-KD) or both (AB-KD) with specific siRNAs (see Materials and Methods). Knocked-down cells were transiently transfected with HA-ClC-2 (see Materials and Methods).

(A) Procedure to sequentially immunolabel HA epitope in intact and permeabilized cells, as described in Figure 3A.

B) Surface (green) and total (red) immunolabeling of HA-ClC-2 in fully polarized cells. Note the reduction of surface levels of HA-ClC-2 and consequent increase of its intracellular levels in AB-KD cells.

C) Bars represent surface and intracellular fractions of HA-ClC-2, calculated from confocal images (see Material and Methods for details). Statistically significant

reduction in surface HA-ClC-2 and increase in intracellular HA-ClC-2 was found only in AB-KD cells. Detailed statistical analysis is shown in supplemental Table S7. Bar= 15 μm.

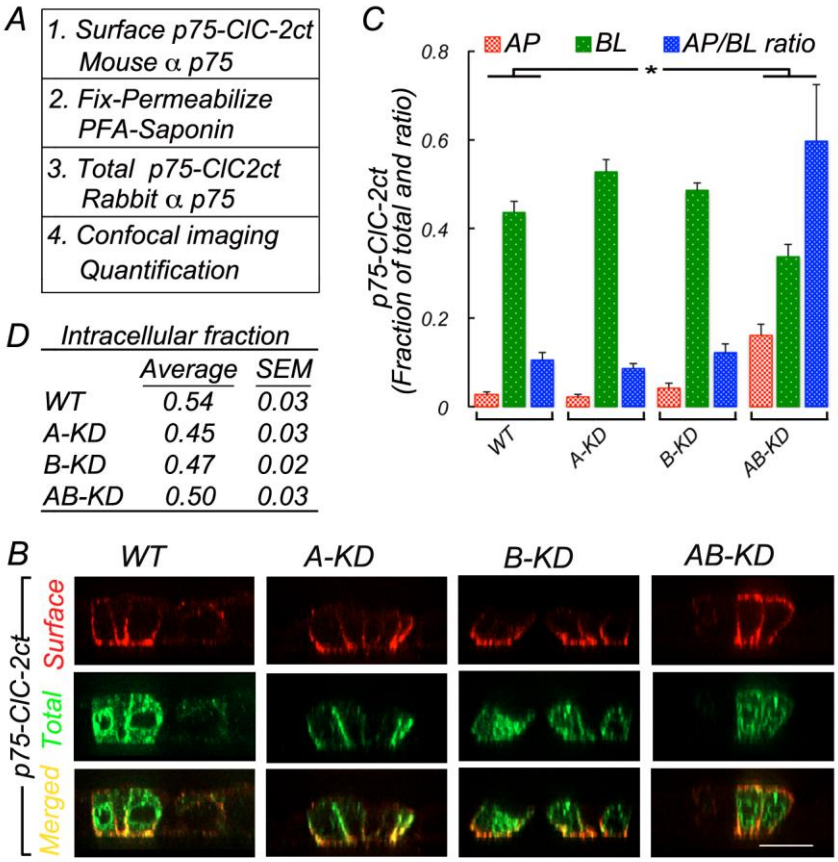

Figure 5. Double knock-down of clathrin adaptors AP-1A and AP-1B promote apical missorting of the p75-ClC-2ct chimera.

MDCK cells permanently expressing the p75-ClC-2ct chimera were silenced for μ1A (A-KD), μ1B (B-KD) or both (AB-KD) with specific siRNAs (see Materials and Methods) and processed for immunofluorescence after 4 days in culture.

A.) Surface and total p75-ClC-2ct sequentially immunolabeled before and after permeabilization with mouse and rabbit anti-p75 antibodies, respectively (see Material and Methods for details).

B) Note that whereas WT, A-KD and B-KD MDCK cells display basolateral localization of p75-ClC-2ct, AB-KD MDCK cells display partial apical redistribution of the chimera.

C) Bars represent fractions of apical (AP) and basolateral (BL) p75-ClC-2ct, calculated from confocal images (see Material and Methods for details) and the A/BL ratio, for each experimental condition. Detailed statistical analysis is shown in supplemental Table S8. Bar= 20 μm

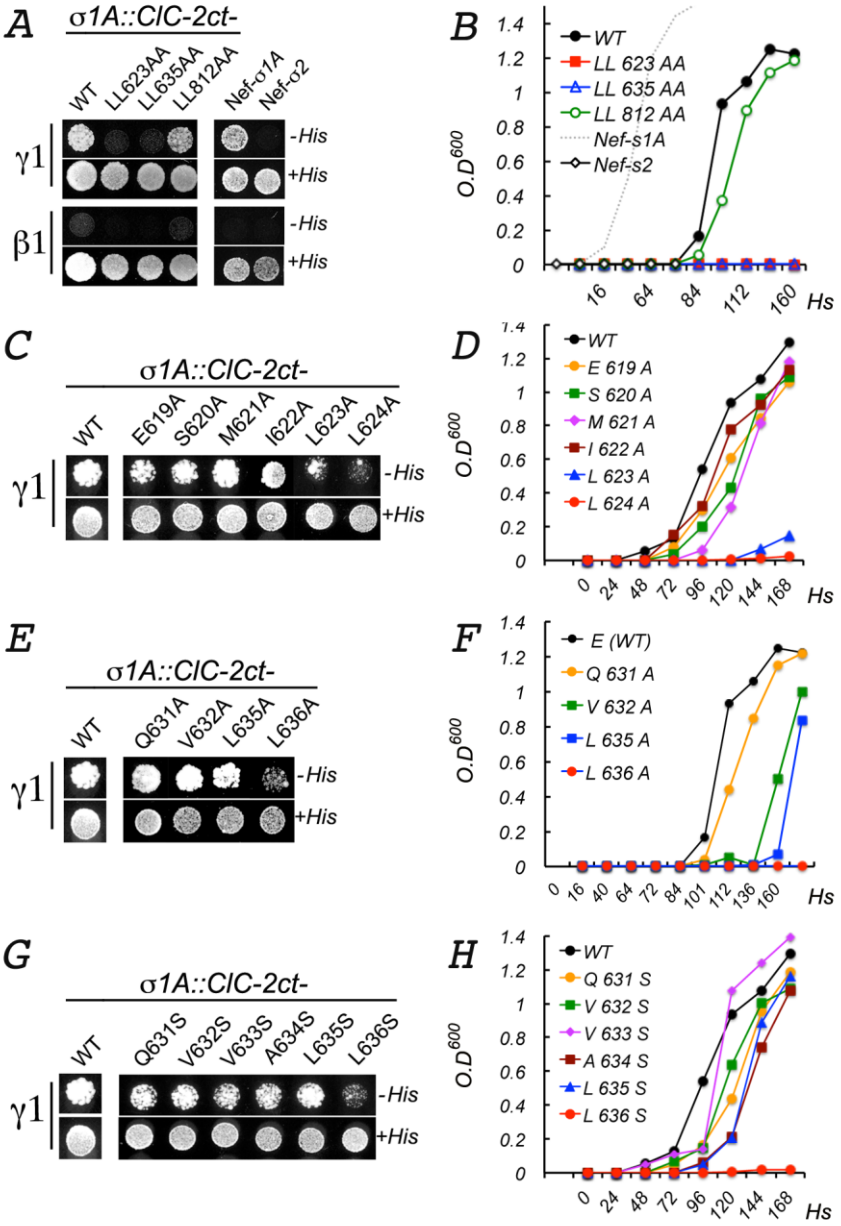

Figure 6. Yeast three hybrid analysis of the interaction between ClC-2ct and AP-1.
The full C-terminus domain (347aa) of ClC-2 (CLC-2ct) and the human σ1A subunit of AP-1 were cloned into different cloning sites of the pBridge vector. The γ1 or β1 subunits were cloned into the pGADT7 vector (see Materials and Methods for details). Growth of co-transformed yeast, reflecting bait/prey interactions, was monitored on plates (A, C, E, G) for 4-6 days or in liquid medium (B, D, F, H) for 0-7 days, in the presence or absence of histidine. Quantification of the interaction in liquid medium (B, D, F, H) was determined by spectrometry at 600nm.

A and B) Wild type ClC-2ct specifically interacted with the γ1-σ1A hemicomplex, although less robustly than Nef (compare black line with dotted gray line in B). Note that ClC-2ct[^{812}LL/AA] interacted with γ1-σ1A (green line) as robustly as WT ClC-2ct (black line). In contrast, ClC-2ct[^{623}LL/AA] and ClC-2ct[^{635}LL/AA] failed to interact with γ1-σ1A .

C and D) Single alanine substitutions in ESMI^{623}LL. The interaction with γ1-σ1A was only blocked by substitutions ^{623}L/A and ^{624}L/A. Note that alanine substitution of the glutamic acid at -4 position did not inhibit the interaction.

E and F) Single alanine substitutions in QVVA^{635}LL. The interaction with γ1-σ1A was only abolished by ^{636}L/A.

G and H) Single serine substitutions QVVA^{635}LL. The interaction with γ1-σ1A was only abolished by ^{636}L/S.

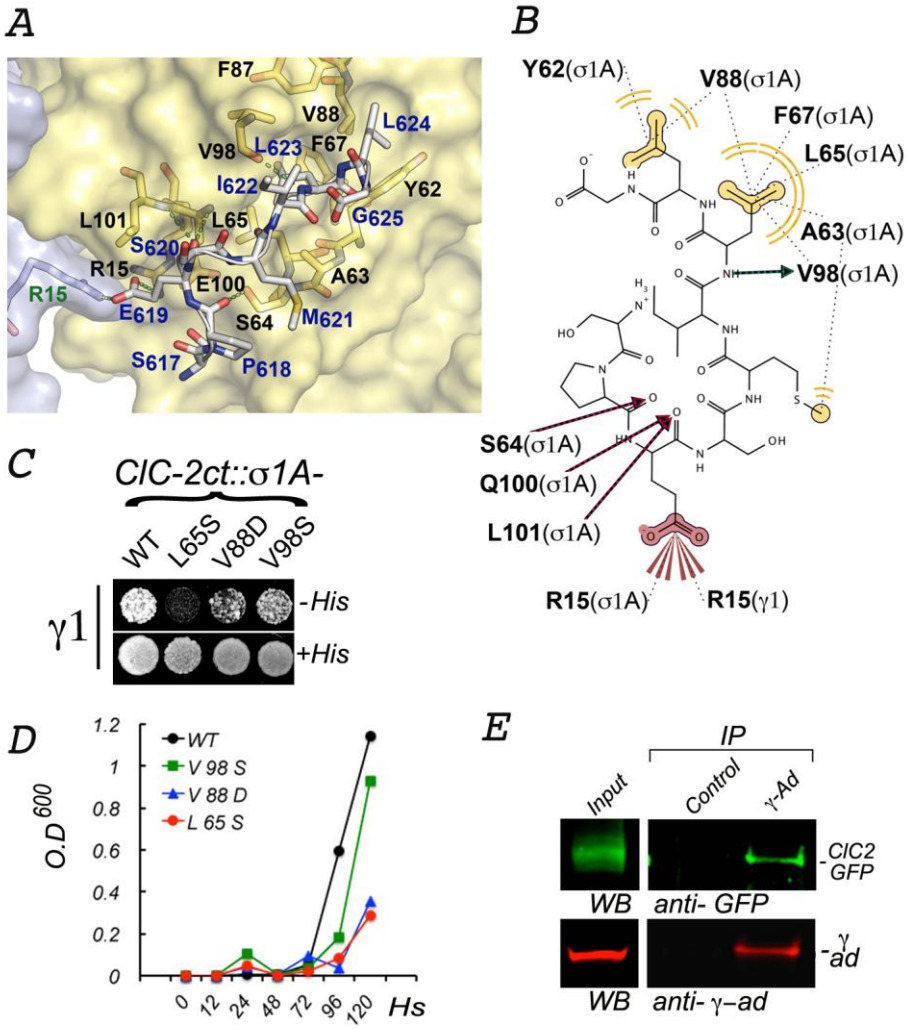

Figure 7. Interactions between ESMI^{623}LL and a conserved pocket in γ1-σ1A

A) In silico model of the interaction between ESMI^{623}LL and γ1-σ1A.
The structure of the γ1-σ1A pocket of AP-1 that interacts with ESMI^{623}LL was modeled from the crystal structure of the corresponding pocket in the α–σ2 hemicomplex of AP-2 (2JKR) (see Materials and Methods). The names of the key pocket residues in the surface-rendered yellow representation of σ1A (in black font) and grey representation of γ1 (in green font) are shown as yellow and orange sticks. The residues in ESMI^{623}LL (labeled in blue font), superimposed on the pocket, are shown in gray sticks with oxygen atoms in red and nitrogen atoms in blue.

B) 2D representation of the interaction of ESMI^{623}LL with the γ1-σ1A pocket. The model shows the leucine residues in ESMI^{623}LL coordinating with σ1 hydrophobic residues (^{62}Y, ^{65}L, ^{67}Phe, ^{88}V and ^{98}V), while the negatively charged residue ^{619}E at -4 position coordinates with positively charged residues ^{15}R in σ1 and ^{15}R in γ1.

C and D) Yeast three hybrid assay shows that interaction of CLC-2ct with γ1-σ1A is inhibited by mutations of two of the residues predicted to be involved in the interaction (^{65}L, ^{88}V).

E) Co-immunoprecipitation of ClC-2-GFP and AP-1. Upon immune-precipitation with mouse γ-adaptin antibodies, the presence of both ClC-2-GFP and γ-adaptin in the precipitate is observed by Western blot.

Table 1. Proteins with dileucine-based basolateral sorting signals

Protein	BL signal &key residues	Endocytic Activity	BL sorting machinery	References
ClC-2	*TIFS**LL***	*?*	*AP-1B*	*Peña-Münzenmayer et al., 2005*
ClC-2	*ESMI**LL***	*?*	*AP-1A, AP-1B*	*This paper*
IgG Fc Receptor B-cell 1 (FcRII-B1)	*ITYS**LL***	*yes*	*?*	*(Hunziker & Fumey, 1994)*
Neonatal IgG-Fc Receptor (FcRn)	***D**SGD**LL***	*yes*	*?*	*Newton et al., 2005*
Glycine Transporter 1b (GLYT 1b)	*DGDT**LL***	*?*	*?*	*Poyatos et al., 2000*
Lutheran antigen(Lu)	*EQTG**LL***	*?*	*?*	*Nemer et al., 1999*
Melanoma cell adhesion molecule isoform 1(MCam-1)	*EEAG**LL***	*?*	*?*	*Guezguez et al., 2006*
Cu^{++} translocating ATPase (ATP7A)	*DKHS**LL***	*?*	*?*	*Greenough et al.,2004*
MHC Class II Invariant chain (MHC-Ii)	*DQRDLL* *EQLPM**L***	*?* *?*	*?*	*Simonsen et al., 1997*
E-cadherin	*VKEP**LL***	*?*	*PIPK-1γ* *AP-1B*	*Miranda et al., 2001* *Ling et al., 2007*
IgG Fc Receptor B-cell 1 (FcRII-B1)	*ITYS**LL***	*yes*	*?*	*(Hunziker & Fumey, 1994)*
Glycoprotein 130 (GP130)	*STQT**LL***	*yes*	*?*	*Doumanov et al., 2006*
Ectonucleotide pyrophosphatase/ phosphodiesterase 1 (NPP1)	*AAAS**LL***	*yes*	*?*	*Bello et al., 2001*
Rat Sulfate anion transporter 1 (SAT-1)	*TAEE**LL***	*yes*	*?*	*Regeer & Markovich 2004*

NCBI sequences of [D/E]XXXL[L/I] dileucine motifs in the cytoplasmic domain of indicated transmembrane cargo proteins. Critical residues for basolateral sorting are highlighted in bold.

Table 2. Residue and residue side-chain solvent area in the three dileucine motifs of ClC-2.

Surface area of	Residue /motif						Total	Norm
	-4	-3	-2	-1	0	1		
	E	S	M	I	L	L		
Residue	134.1	72.2	46.7	16.1	36.8	60.3	366.3	1.0
Side chain	126.5	62.1	45.5	16.1	26.7	51.5	328.4	1.0
	Q	V	V	A	L	L		
Residue	116.4	0.6	37.8	60.2	34.9	13.0	262.7	0.7
Side chain	107.3	0.6	34.3	40.9	34.9	13.0	230.9	0.7
	T	I	F	S	L	L		
Residue	52.8	13.0	0.3	26.3	101.5	62.2	256.2	0.7
Side chain	48.1	10.8	0.3	21.3	87.0	41.2	208.7	0.6

The averages of solvent accessibilities values, per residue and side-chain, corresponding to each motif's residue expressed in $Å^2$ were determined with Discovery Studio v2.1 (Accelrys Inc., San Diego) software. Total values for each parameter measured were normalized to values corresponding to $ESMI^{623}LL$ motif.